Supporting Information for

Cell Adhesion Proteins Modulate the Carbon Nanotube Optical Bandgap *via* Surface Charge Accumulation

*Daniel Roxbury[1], Prakrit V. Jena[1], Yosi Shamay[1], Christopher P. Horoszko[1,2], and Daniel A. Heller[1,2]**

[1]Memorial Sloan-Kettering Cancer Center, New York, NY, USA.
[2]Weill Cornell Medical College, New York, NY, USA.

Supporting Figures

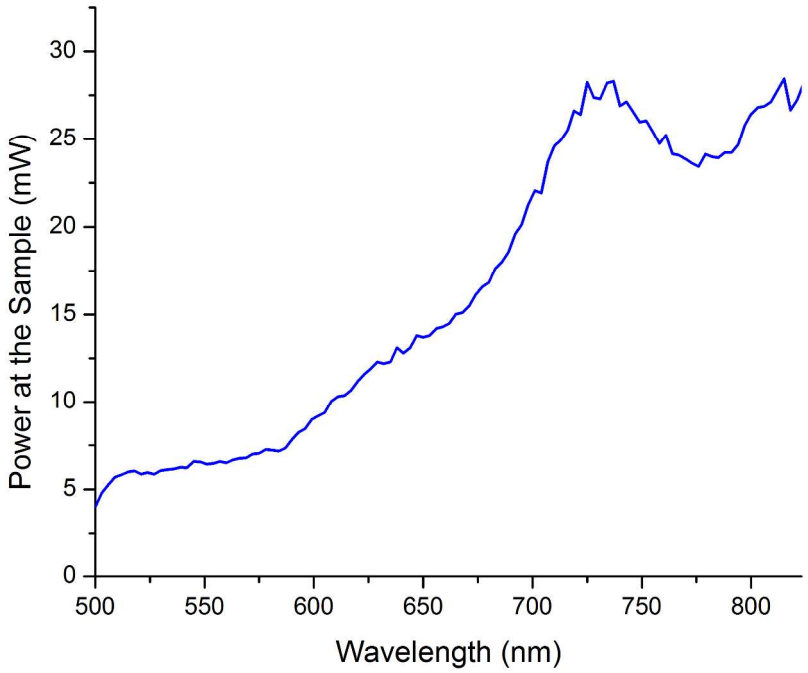

Figure S1. Excitation power measured through a 50x objective at the location of the sample.

To correct for wavelength-dependent variations in excitation efficiency of the supercontinuum laser/bandpass filter, the excitation power was measured at the sample (ThorLabs PM100D power meter). The excitation power calibration curve is shown in Figure S1. The measured power values were used to apply a correction factor at each excitation wavelength between 500 and 827 mm (20 nm bandwidth, 3 nm steps).

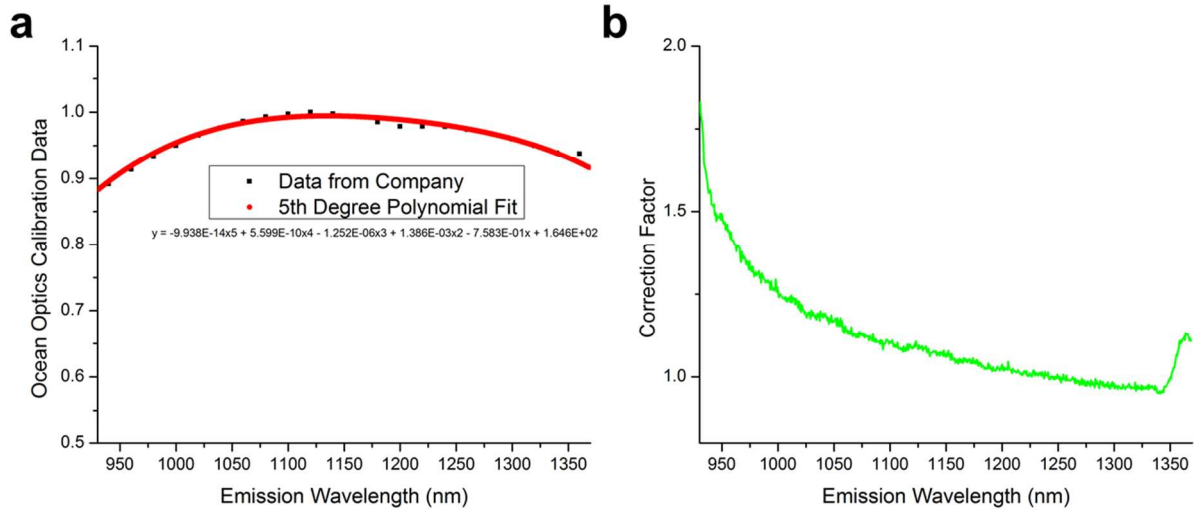

Figure S2. Emission intensity calibration. (a) Halogen calibration light source data provided by the manufacturer and 5th degree polynomial least-squares fit. (b) Emission calibration curve collected through a 50x objective.

An HL-3-CAL-EXT halogen calibration light source (Ocean Optics) was used to correct for wavelength-dependent grating, detector, and lenses/mirror efficiencies. Calibration data provided by the lamp manufacturer was fit to a 5th degree polynomial over the range of emission wavelengths used in the experiments (Figure S2). An Hg/Ne lamp (Newport) was used to calibrate spectrometer wavelength in the 930-1370 nm range.[1]

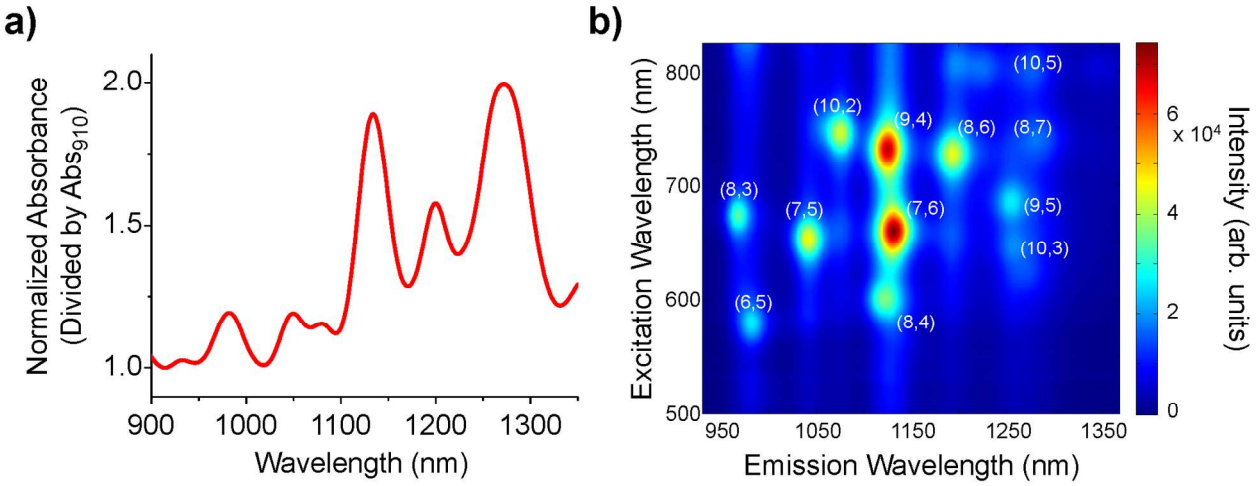

Figure S3. Spectroscopic characterization of the ss(AT)$_{15}$-HiPco nanotube complex. (a) Absorbance scan of ss(AT)$_{15}$-HiPco nanotube complexes diluted in cellular media without serum. The data has been normalized at 910 nm. (b) Photoluminescence plot of ss(AT)$_{15}$-HiPco complexes diluted in cell media without serum. Nanotube (n,m) species (chiralities) are labeled.

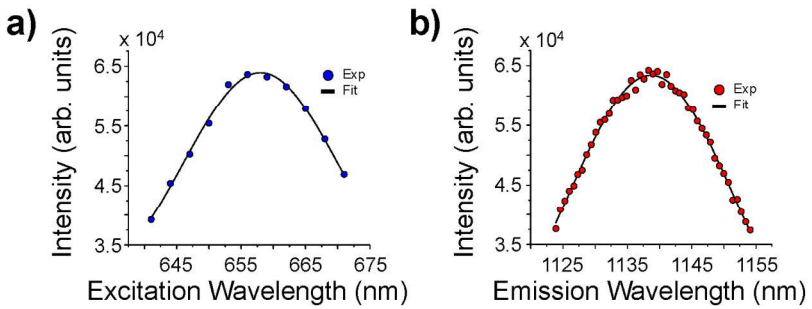

Figure S4. Sample Gaussian fits of nanotube photoluminescence spectra. (a) Excitation spectrum of the (7,6)-nanotube extracted from the two-dimensional photoluminescence plot of ss$(AT)_{15}$-HiPco nanotubes. The line is a Gaussian fit of the form: Intensity = $Intensity_0$ + Area*exp(-0.5*((λ-λc)/w^2) (b) Emission spectrum and Gaussian fit of the same (7,6) nanotube.

To extract λ_{11} and λ_{22} values for 12 observed nanotube (n,m) species from excitation/emission spectra, code was written to use initial guesses of the excitation and emission maxima. Individual peaks were sequentially fit with Gaussian lineshapes using a least-squares algorithm to ascertain the center excitation and emission wavelengths.

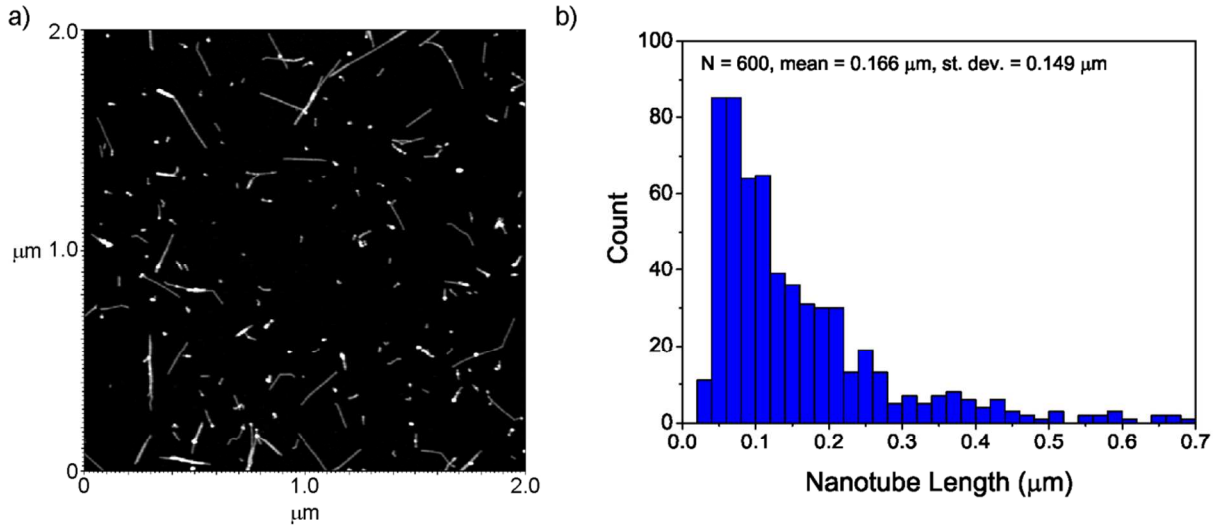

Figure S5. Length characterization of nanotubes by atomic force microscopy. (a) Representative micrograph of the ss(AT)15-HiPco sample deposited onto a freshly-cleaved mica surface. (b) Length distribution histogram incorporating length information from 600 nanotubes. Bin size equals 0.02 μm.

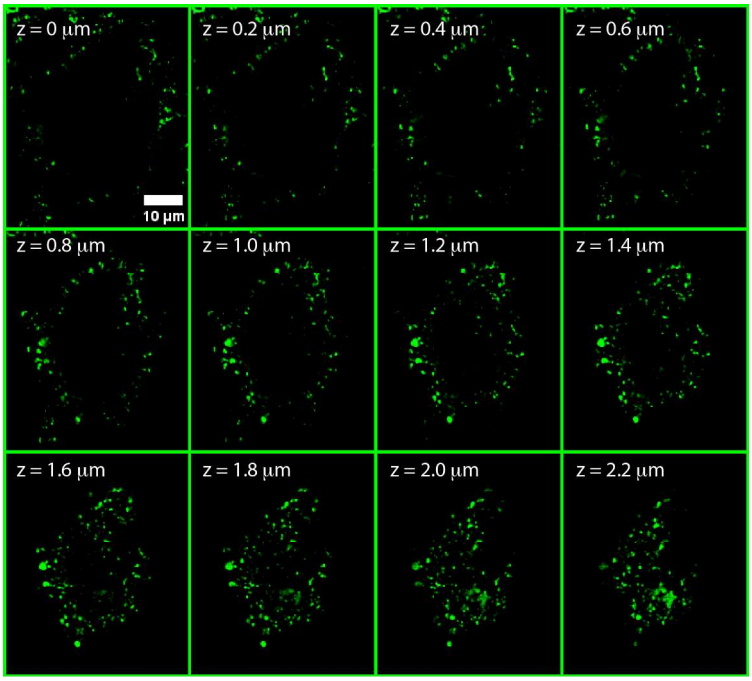

Figure S6. Deconvolved nIR broadband fluorescence images (900-1600 nm) of increasing height from the culture dish surface acquired from a HeLa cell incubated with 5 mg/L ss$(AT)_{15}$-HiPco nanotubes for 5 minutes.

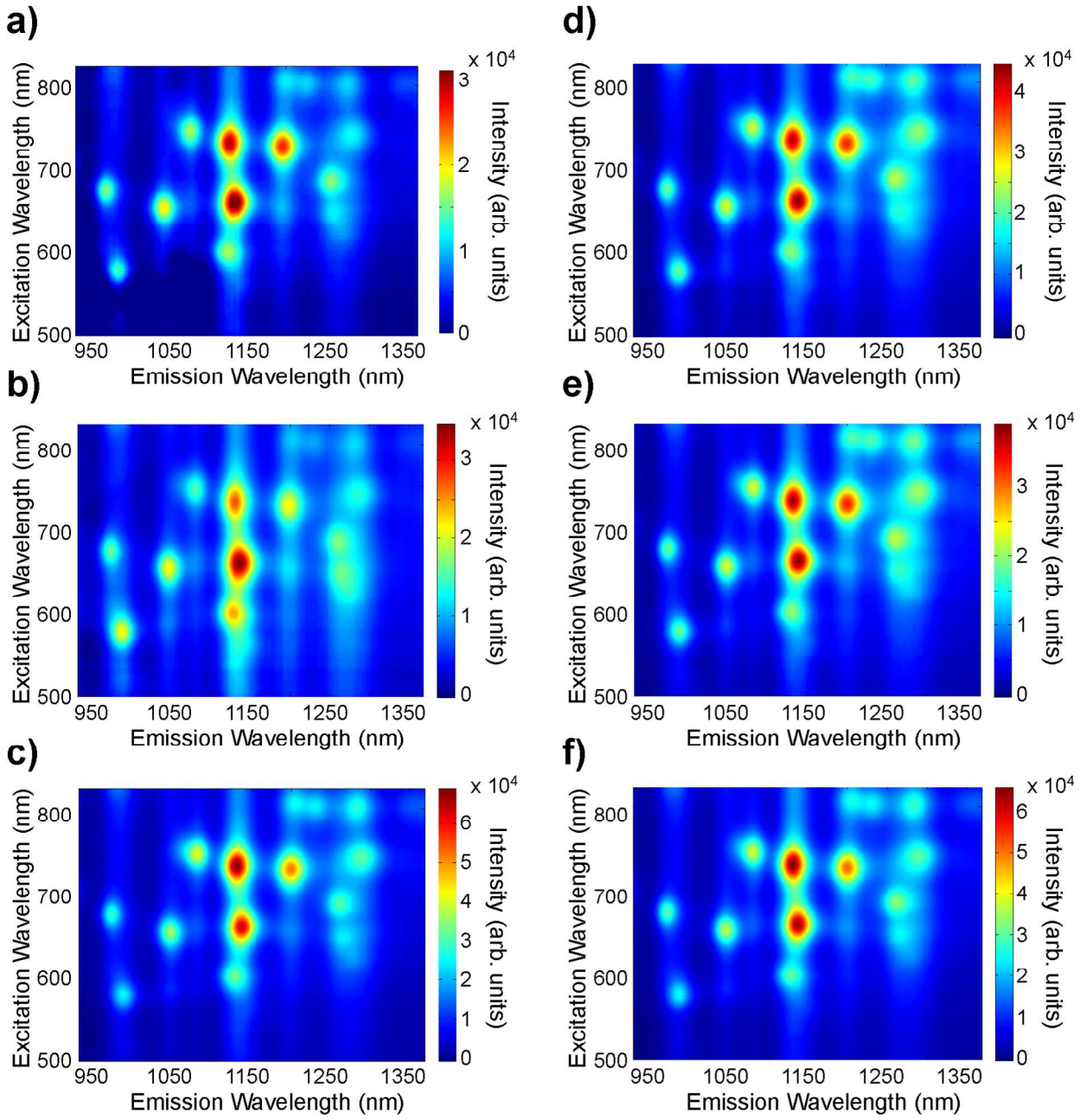

Figure S7. Photoluminescence plots of ss$(AT)_{15}$-HiPco nanotube complexes on cell membranes before and after trypsinization. (a) Representative data from ss$(AT)_{15}$-HiPco nanotubes on the surface of adherent HeLa cells, (b) adherent NIH/3T3 cells, (c) Jurkat cells in a native suspension state. (d) Representative data from ss$(AT)_{15}$-HiPco nanotubes on the surface of trypsinized HeLa cells, (b) on trypsinized NIH/3T3 cells, and (c) on trypsinized Jurkat cells.

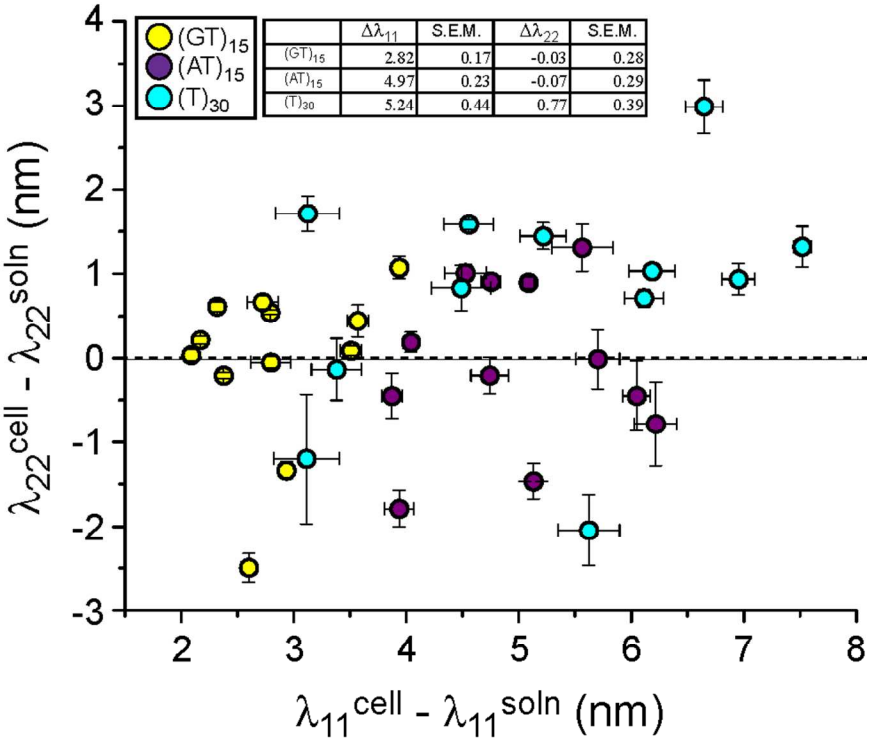

	Δλ11	S.E.M.	Δλ22	S.E.M.
$(GT)_{15}$	2.82	0.17	-0.03	0.28
$(AT)_{15}$	4.97	0.23	-0.07	0.29
$(T)_{30}$	5.24	0.44	0.77	0.39

Figure S8. Photoluminescence responses of $ss(GT)_{15}$, $ss(AT)_{15}$, and $ss(T)_{30}$-HiPco nanotube complexes to the native NIH/3T3 cell surface. The fitted emission peak wavelengths are plotted relative to values from nanotube complexes in solution (cell media without serum, denoted soln). Error bars represent S.E.M., n=5.

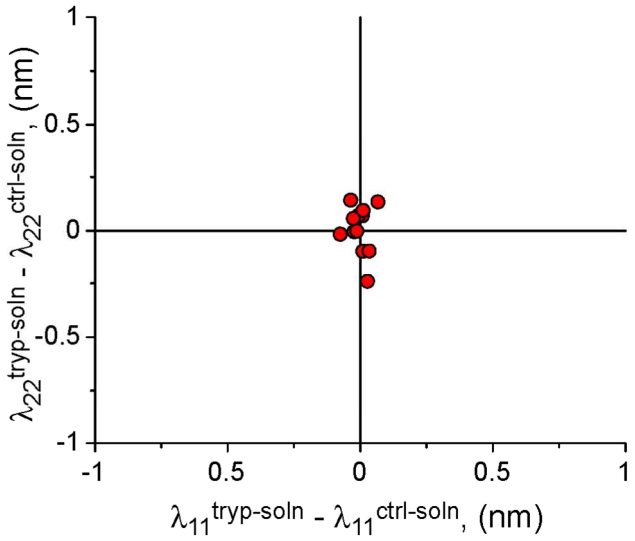

Figure S9. Control experiment to assess nanotube response to trypsin in solution. Fitted center excitation and emission wavelengths from $ss(AT)_{15}$-HiPco in cell culture media containing trypsin (10% of stock) minus control (cell culture media without trypsin).

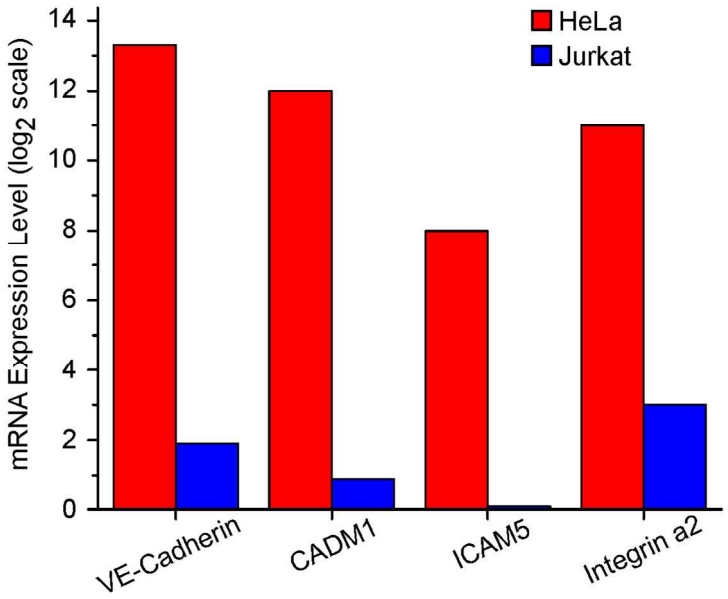

Figure S10. mRNA expression levels of adhesion molecules on HeLa and Jurkat cells, from the Broad-Novartis Cancer Cell Line Encyclopedia.

The Broad-Novartis Cancer Cell Line Encyclopedia is a compilation of gene expression data from 947 human cancer cell lines.[2] As HeLa and Jurkat cell lines are derived from human patient samples, mRNA expression levels for these two cell types are included in the encyclopedia. Comparing four types of cellular adhesion proteins, it is clear that HeLa cell expression of these proteins is much higher than Jurkat cells.

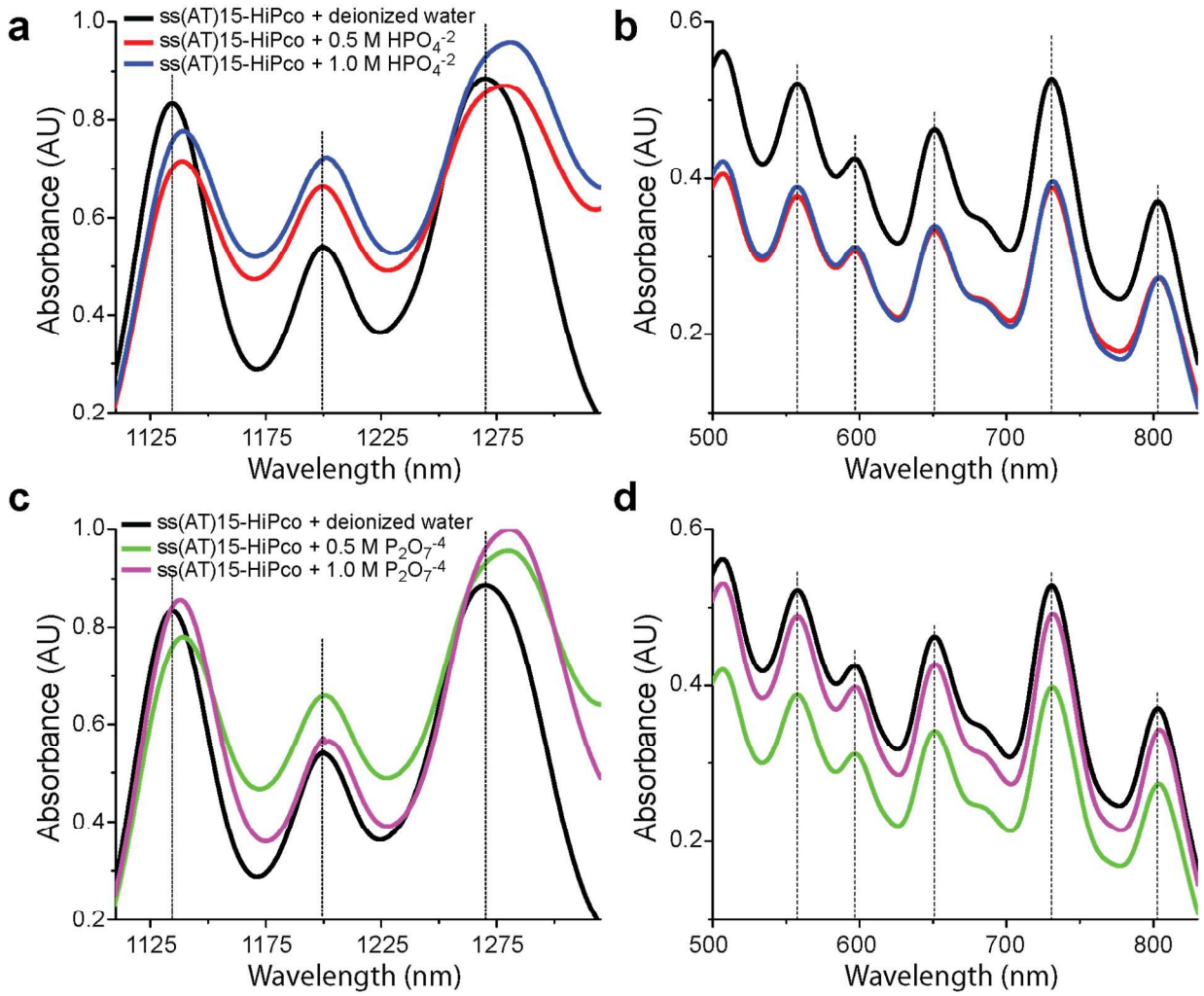

Figure S11. Absorbance spectra of ss(AT)$_{15}$-HiPco nanotube spectra in phosphate solutions. (a) Monophosphates, at 0.5 or 1 M, red-shifted nanotube λ_{11} absorbance bands. Black vertical lines are for visual reference to the sample in deionized water. (b) λ_{22} absorbance bands showed little or no response to added monophosphates. (c) Pyrophosphates, at 0.5 or 1 M, also shifted nanotube λ_{11} absorbance bands. (d) λ_{22} absorbance bands again showed little or no response to added pyrophosphates.

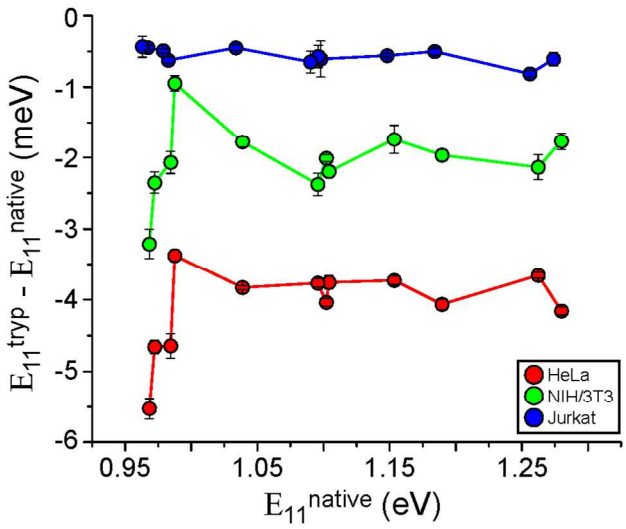

Figure S12. Scatter plot between nanotube emission energy change (between trypsinized and native states, E_{11}tryp-E_{11}native) versus nanotube emission energy for HeLa, NIH/3T3, and Jurkat cells.

Table S1. Fitted λ_{11} and λ_{22} values, along with goodness of fit values (adjusted R^2), as a function of chirality, for ss$(AT)_{15}$-HiPco nanotubes in cell culture media without serum.

Chirality (n,m)	λ_{11} (nm)	Fit R^2	λ_{22} (nm)	Fit R^2
(8,3)	968.78	0.988	673.22	0.999
(6,5)	982.36	0.989	579.55	0.995
(7,5)	1042.29	0.994	652.87	0.994
(10,2)	1074.94	0.984	745.14	0.999
(8,4)	1123.04	0.976	601.04	0.989
(9,4)	1125.14	0.998	730.62	0.998
(7,6)	1131.60	0.996	659.72	0.997
(8,6)	1193.74	0.997	726.66	0.999
(9,5)	1255.68	0.979	684.72	0.997
(10,3)	1259.48	0.938	648.65	0.945
(10,5)	1275.28	0.944	800.09	0.989
(8,7)	1280.43	0.955	739.92	0.988

Table S2. Fitted λ_{11} and λ_{22} values, along with goodness of fit values (adjusted R^2), as a function of chirality, for ss$(AT)_{15}$-HiPco nanotubes on the surface of adherent HeLa cells. Note, λ_{22} values for the (10,3) nanotube have been omitted from plots and calculations due to bad goodness of fits.

Chirality (n,m)	λ_{11} (nm) 1	Fit R^2 1	λ_{22} (nm) 1	Fit R^2 1	λ_{11} (nm) 2	Fit R^2 2	λ_{22} (nm) 2	Fit R^2 2	λ_{11} (nm) 3	Fit R^2 3	λ_{22} (nm) 3	Fit R^2 3
(8,3)	970.91	0.973	673.56	0.969	970.76	0.977	673.80	0.996	970.85	0.984	674.00	0.991
(6,5)	985.09	0.923	580.53	0.954	985.05	0.964	579.41	0.952	984.97	0.961	579.02	0.980
(7,5)	1044.29	0.978	652.82	0.985	1044.58	0.984	652.90	0.987	1044.65	0.984	652.88	0.975
(10,2)	1077.47	0.989	744.71	0.993	1077.80	0.991	745.19	0.996	1077.61	0.993	744.92	0.996
(8,4)	1126.88	0.952	600.21	0.950	1126.58	0.941	601.14	0.981	1126.34	0.972	600.18	0.984
(9,4)	1128.13	0.994	730.71	0.999	1128.06	0.995	731.11	0.997	1128.12	0.997	731.04	0.999
(7,6)	1134.76	0.989	659.30	0.989	1134.99	0.989	659.55	0.992	1134.86	0.993	659.42	0.987
(8,6)	1195.97	0.992	726.81	0.998	1196.08	0.994	726.93	0.996	1196.07	0.996	727.00	0.998
(9,5)	1258.10	0.935	685.02	0.968	1258.35	0.952	685.09	0.988	1258.58	0.947	684.89	0.988
(10,3)	1262.17	0.782	651.37	0.464	1261.76	0.875	651.33	0.202	1262.43	0.887	652.10	0.292
(10,5)	1277.61	0.933	799.74	0.941	1277.92	0.929	799.66	0.911	1278.28	0.955	799.50	0.969
(8,7)	1282.34	0.920	740.21	0.973	1282.79	0.913	740.94	0.987	1283.36	0.929	740.35	0.971

Chirality (n,m)	λ_{11} (nm) 4	Fit R^2 4	λ_{22} (nm) 4	Fit R^2 4	λ_{11} (nm) 5	Fit R^2 5	λ_{22} (nm) 5	Fit R^2 5
(8,3)	970.68	0.984	673.58	0.997	970.90	0.979	673.96	0.990
(6,5)	984.96	0.960	579.11	0.881	985.11	0.971	578.68	0.968
(7,5)	1044.49	0.985	652.96	0.992	1044.56	0.988	653.28	0.986
(10,2)	1077.51	0.990	745.04	0.998	1077.59	0.992	745.52	0.996
(8,4)	1126.50	0.951	600.35	0.985	1126.75	0.953	600.87	0.974
(9,4)	1128.02	0.996	730.82	0.998	1128.35	0.997	731.19	0.998
(7,6)	1134.89	0.991	659.35	0.994	1135.10	0.991	659.75	0.995
(8,6)	1196.05	0.996	726.96	0.999	1196.17	0.996	727.09	0.999

(9,5)	1258.21	0.952	684.93	0.992	1258.55	0.956	684.74	0.995
(10,3)	1262.27	0.944	649.91	0.626	1263.09	0.894	648.94	0.918
(10,5)	1277.82	0.944	799.33	0.972	1278.06	0.942	799.45	0.938
(8,7)	1283.11	0.951	740.11	0.988	1283.37	0.946	740.79	0.988

Table S3. Fitted λ_{11} and λ_{22} values, along with goodness of fit values (adjusted R^2), as a function of chirality, for ss$(AT)_{15}$-HiPco nanotubes on the surface of adherent NIH/3T3 cells.

Chirality (n,m)	**λ_{11} (nm) 1**	**Fit R^2 1**	**λ_{22} (nm) 1**	**Fit R^2 1**	**λ_{11} (nm) 2**	**Fit R^2 2**	**λ_{22} (nm) 2**	**Fit R^2 2**	**λ_{11} (nm) 3**	**Fit R^2 3**	**λ_{22} (nm) 3**	**Fit R^2 3**
(8,3)	972.48	0.971	672.65	0.969	972.45	0.978	671.88	0.969	972.94	0.982	672.73	0.995
(6,5)	985.96	0.935	578.04	0.933	986.02	0.890	578.23	0.952	986.60	0.976	577.36	0.979
(7,5)	1046.28	0.980	652.95	0.972	1046.55	0.975	653.08	0.968	1046.18	0.991	652.65	0.992
(10,2)	1079.49	0.968	745.84	0.984	1080.12	0.984	746.13	0.993	1079.01	0.983	746.10	0.994
(8,4)	1128.03	0.930	599.03	0.969	1128.18	0.955	600.09	0.968	1128.39	0.979	599.44	0.990
(9,4)	1130.24	0.990	731.54	0.991	1130.42	0.991	731.50	0.996	1130.21	0.994	731.34	0.993
(7,6)	1136.22	0.975	659.81	0.983	1136.92	0.981	659.42	0.990	1135.93	0.991	658.80	0.993
(8,6)	1198.31	0.988	727.34	0.977	1198.80	0.990	727.64	0.994	1198.40	0.996	727.41	0.997
(9,5)	1261.27	0.938	684.19	0.964	1261.72	0.935	685.36	0.993	1262.01	0.950	682.84	0.985
(10,3)	1266.42	0.748	646.82	0.902	1265.69	0.919	648.15	0.857	1265.44	0.960	646.61	0.935
(10,5)	1280.72	0.898	799.90	0.923	1281.64	0.958	800.91	0.980	1280.51	0.960	798.84	0.968
(8,7)	1285.88	0.870	740.86	0.969	1286.66	0.926	741.85	0.974	1285.15	0.951	740.56	0.982

Chirality (n,m)	**λ_{11} (nm) 4**	**Fit R^2 4**	**λ_{22} (nm) 4**	**Fit R^2 4**	**λ_{11} (nm) 5**	**Fit R^2 5**	**λ_{22} (nm) 5**	**Fit R^2 5**
(8,3)	972.68	0.984	673.49	0.983	972.71	0.981	673.10	0.981
(6,5)	986.51	0.958	578.06	0.947	986.37	0.979	577.13	0.990
(7,5)	1046.44	0.989	653.24	0.993	1046.22	0.992	653.36	0.995
(10,2)	1079.47	0.984	746.42	0.988	1079.23	0.984	746.30	0.991

(8,4)	1127.99	0.960	600.04	0.956	1128.25	0.979	599.29	0.985
(9,4)	1130.18	0.993	731.75	0.994	1130.11	0.995	731.47	0.998
(7,6)	1136.46	0.986	660.09	0.994	1136.20	0.990	659.45	0.992
(8,6)	1198.52	0.995	727.83	0.996	1198.40	0.996	727.60	0.997
(9,5)	1261.80	0.945	684.74	0.988	1261.82	0.969	684.22	0.979
(10,3)	1265.45	0.941	649.16	0.874	1265.45	0.964	648.59	0.907
(10,5)	1281.08	0.953	800.51	0.991	1280.97	0.969	800.24	0.990
(8,7)	1286.50	0.977	741.93	0.978	1285.75	0.962	740.92	0.987

Table S4. Fitted λ_{11} and λ_{22} values, along with goodness of fit values (adjusted R^2), as a function of chirality, for ss$(AT)_{15}$-HiPco nanotubes on the surface Jurkat cells.

Chirality (n,m)	**λ_{11} (nm) 1**	**Fit R^2 1**	**λ_{22} (nm) 1**	**Fit R^2 1**	**λ_{11} (nm) 2**	**Fit R^2 2**	**λ_{22} (nm) 2**	**Fit R^2 2**	**λ_{11} (nm) 3**	**Fit R^2 3**	**λ_{22} (nm) 3**	**Fit R^2 3**
(8,3)	973.41	0.993	673.97	0.993	973.45	0.992	673.69	0.998	973.54	0.993	673.69	0.999
(6,5)	987.21	0.985	578.36	0.990	987.10	0.993	576.89	0.998	987.14	0.995	577.18	0.995
(7,5)	1047.35	0.993	652.94	0.993	1047.29	0.995	652.93	0.996	1047.37	0.994	653.38	0.996
(10,2)	1080.09	0.987	745.81	0.995	1080.02	0.986	746.17	0.997	1080.07	0.986	745.87	0.996
(8,4)	1129.29	0.975	601.29	0.993	1129.59	0.982	600.13	0.996	1129.74	0.981	599.89	0.993
(9,4)	1131.13	0.999	731.82	0.999	1131.30	0.999	731.83	0.999	1131.42	0.999	731.54	0.997
(7,6)	1137.25	0.997	659.49	0.998	1137.44	0.998	659.42	0.996	1137.53	0.999	659.88	0.996
(8,6)	1199.56	0.998	727.87	0.999	1199.42	0.999	727.83	0.999	1199.48	0.999	727.67	0.998
(9,5)	1262.10	0.979	686.59	0.993	1262.10	0.981	685.48	0.994	1262.17	0.983	685.22	0.999
(10,3)	1267.10	0.938	648.27	0.971	1266.99	0.945	648.07	0.979	1267.04	0.946	648.70	0.951
(10,5)	1282.47	0.987	800.75	0.990	1282.35	0.984	800.70	0.986	1282.35	0.985	801.21	0.989
(8,7)	1287.97	0.988	741.43	0.994	1287.47	0.986	741.51	0.994	1287.56	0.988	740.96	0.990

Table S5. Fitted λ_{11} and λ_{22} values, along with goodness of fit values (adjusted R^2), as a function of chirality, for ss$(AT)_{15}$-HiPco nanotubes on the surface of trypsinized HeLa cells in suspension.

Chirality (n,m)	λ_{11} (nm) 1	Fit R^2 1	λ_{22} (nm) 1	Fit R^2 1	λ_{11} (nm) 2	Fit R^2 2	λ_{22} (nm) 2	Fit R^2 2	λ_{11} (nm) 3	Fit R^2 3	λ_{22} (nm) 3	Fit R^2 3
(8,3)	973.98	0.992	674.15	0.993	973.99	0.990	674.08	0.996	973.96	0.989	674.39	0.996
(6,5)	987.90	0.981	577.09	0.993	987.89	0.982	577.33	0.992	987.89	0.982	577.00	0.982
(7,5)	1048.11	0.989	653.44	0.995	1048.08	0.990	653.36	0.999	1048.08	0.990	653.43	0.998
(10,2)	1081.05	0.987	746.71	0.996	1081.11	0.985	746.70	0.995	1081.09	0.985	746.81	0.994
(8,4)	1130.44	0.944	600.15	0.977	1130.47	0.964	600.53	0.988	1130.43	0.944	600.00	0.996
(9,4)	1132.26	0.996	731.91	0.998	1132.27	0.996	731.73	0.997	1132.28	0.996	731.85	0.999
(7,6)	1138.79	0.992	660.21	0.998	1138.83	0.993	660.25	0.998	1138.85	0.992	660.27	0.999
(8,6)	1200.50	0.995	727.96	0.999	1200.48	0.996	727.61	0.999	1200.48	0.995	728.06	0.991
(9,5)	1262.63	0.971	686.12	0.990	1262.61	0.968	686.00	0.993	1262.76	0.957	686.27	0.997
(10,3)	1268.30	0.860	649.43	0.924	1268.32	0.860	650.19	0.947	1268.32	0.856	650.18	0.909
(10,5)	1284.00	0.977	801.47	0.988	1284.06	0.979	801.13	0.995	1284.17	0.975	801.21	0.990
(8,7)	1290.29	0.975	741.86	0.994	1290.37	0.975	741.91	0.994	1290.36	0.971	742.09	0.996

Table S6. Fitted λ_{11} and λ_{22} values, along with goodness of fit values (adjusted R^2), as a function of chirality, for ss$(AT)_{15}$-HiPco nanotubes on the surface of trypsinized NIH/3T3 cells in suspension.

Chirality (n,m)	λ_{11} (nm) 1	Fit R^2 1	λ_{22} (nm) 1	Fit R^2 1	λ_{11} (nm) 2	Fit R^2 2	λ_{22} (nm) 2	Fit R^2 2	λ_{11} (nm) 3	Fit R^2 3	λ_{22} (nm) 3	Fit R^2 3
(8,3)	974.00	0.989	674.20	0.995	974.01	0.989	674.08	0.997	973.97	0.989	674.17	0.997
(6,5)	987.94	0.982	576.98	0.993	988.06	0.982	577.07	0.988	987.86	0.985	577.28	0.988
(7,5)	1048.07	0.987	653.69	0.996	1048.08	0.987	653.41	0.992	1048.02	0.987	653.51	0.997
(10,2)	1081.07	0.985	746.54	0.996	1081.11	0.987	746.53	0.994	1081.08	0.985	746.62	0.994
(8,4)	1130.48	0.955	599.94	0.993	1130.40	0.949	599.88	0.969	1130.34	0.951	599.96	0.992
(9,4)	1132.27	0.995	731.67	0.999	1132.29	0.995	731.59	0.997	1132.29	0.995	731.87	0.998
(7,6)	1138.77	0.990	660.11	0.999	1138.81	0.992	660.15	0.998	1138.83	0.989	660.20	0.996
(8,6)	1200.53	0.995	727.64	0.999	1200.53	0.994	727.62	0.999	1200.53	0.995	727.99	0.998
(9,5)	1263.01	0.957	685.84	0.997	1262.82	0.971	686.10	0.990	1262.96	0.963	686.28	0.996
(10,3)	1268.31	0.857	650.20	0.966	1268.26	0.887	649.37	0.891	1268.46	0.866	649.49	0.880
(10,5)	1284.03	0.978	801.22	0.985	1284.12	0.978	801.25	0.993	1284.09	0.979	801.38	0.991
(8,7)	1290.15	0.970	741.69	0.991	1290.29	0.976	741.73	0.991	1290.31	0.970	741.85	0.994

Table S7. Fitted λ_{11} and λ_{22} values, along with goodness of fit values (adjusted R^2), as a function of chirality, for ss$(AT)_{15}$-HiPco nanotubes on the surface of trypsinized Jurkat cells in suspension.

Chirality (n,m)	λ_{11} (nm) 1	Fit R^2 1	λ_{22} (nm) 1	Fit R^2 1	λ_{11} (nm) 2	Fit R^2 2	λ_{22} (nm) 2	Fit R^2 2	λ_{11} (nm) 3	Fit R^2 3	λ_{22} (nm) 3	Fit R^2 3
(8,3)	973.82	0.992	674.36	0.998	973.98	0.991	673.94	0.996	974.01	0.991	673.87	0.996
(6,5)	987.76	0.986	577.87	0.993	987.82	0.991	577.12	0.996	987.80	0.994	577.37	0.996
(7,5)	1047.71	0.992	653.72	0.995	1047.81	0.992	653.32	0.995	1047.82	0.993	653.49	0.995
(10,2)	1080.56	0.987	745.72	0.998	1080.60	0.986	745.92	0.997	1080.60	0.985	745.44	0.996
(8,4)	1129.72	0.970	600.69	0.996	1130.34	0.975	599.78	0.991	1130.44	0.976	600.41	0.995
(9,4)	1131.60	0.999	731.13	0.998	1131.96	0.999	731.39	0.999	1132.05	0.999	731.11	0.999
(7,6)	1137.82	0.997	660.36	0.995	1138.19	0.998	659.79	0.998	1138.25	0.999	660.16	0.997

(8,6)	1199.97	0.998	727.33	0.999	1200.03	0.999	727.40	0.999	1200.03	0.999	727.26	0.999
(9,5)	1262.81	0.974	686.17	0.999	1262.96	0.977	685.15	0.997	1263.01	0.978	685.86	0.993
(10,3)	1267.63	0.947	650.34	0.921	1267.70	0.954	648.97	0.935	1267.72	0.959	649.09	0.979
(10,5)	1283.01	0.983	801.58	0.978	1282.97	0.981	801.23	0.990	1282.96	0.982	800.95	0.989
(8,7)	1288.45	0.985	740.61	0.991	1288.27	0.988	740.87	0.997	1288.02	0.985	739.72	0.985

References:

1 DeRose, P. C. & Resch-Genger, U. Recommendations for Fluorescence Instrument Qualification: The New ASTM Standard Guide. *Anal. Chem.* **2010**, *82*, 2129-2133.

2 Barretina, J.; Caponigro, G; Stransky, N.; Venkatesan, K.; Margolin, A.; Kim, S.; Wilson, C.J.; Lehár, J.; Kryukov, G.V.; Sonkin, D. *et al*. The Cancer Cell Line Encyclopedia Enables Predictive Modelling of Anticancer Drug Sensitivity. *Nature,* **2012**, *483*, 603-307.